6-14-2023

The Importance of Accurately Predicting Corner Separations in Fan Stall Point Identification with Steady RANS: Computations with The Helicity-Corrected Spalart-Allmaras Turbulence Model

ZHIFAN YU
University of Windsor

The Importance of Accurately Predicting Corner Separations in Fan Stall Point Identification with Steady RANS: Computations with The Helicity-Corrected Spalart-Allmaras Turbulence Model

by

Zhifan Yu

A Thesis
Submitted to the Faculty of Graduate Studies
through the Department of Mechanical, Automotive, and Materials Engineering
in Partial Fulfillment of the Requirements for
the Degree of Master of Applied Science
at the University of Windsor

Windsor, Ontario, Canada

2023

The Importance of Accurately Predicting Corner Separations in Fan Stall Point Identification with Steady RANS: Computations with The Helicity-corrected Spalart-Allmaras Turbulence Model

by

Zhifan Yu

APPROVED BY:

_____

F. Gherib

Department of Civil & Environmental Engineering

_____

N. Eaves

Department of Mechanical, Automotive, and Materials Engineering

_____

J. Defoe, Advisor

Department of Mechanical, Automotive, and Materials Engineering

April 26, 2023

DECLARATION OF CO-AUTHORSHIP / PREVIOUS PUBLICATIONS

I. Co-Authorship

I hereby declare that this thesis incorporates material that is the outcome of joint research, as follows: The thesis was authored by Zhifan Yu under the supervision of Dr. Jeff Defoe, who is also the co-author of the papers published through this work. The other co-author for the paper contained in Chapter 2, Hussain Raza, assisted with carrying out computations. The primary contributions/novelties, data analysis, interpretation, and writing were performed by the author and the contribution of Dr. Jeff Defoe were in providing supervision, feedback, and comments.

I am aware of the University of Windsor Senate Policy on Authorship, and I certify that I have properly acknowledged the contribution of other researchers to my thesis and have obtained written permission from each of the co-author(s) to include the above material(s) in my thesis.

II. Previous Publication

This thesis partly includes original papers that have been previously submitted to conferences, as provided in the following table:

Thesis Chapter	Publication Title/Full Citation	Publication Status
Chapter 2	Z. Yu, H. Raza, J. Defoe, "Assessment of Fan Stall Point Identification Ability of Steady RANS Computations with the Helicity-Corrected Spalart-Allmaras Turbulence Model," Proceedings of *ASME Turbo Expo 2023*, 2023. Paper GT2023-104039.	In press
Chapter 3	Z. Yu, J. Defoe, "Validation of Helicity-Corrected Spalart-Allmaras Model for Corner Separation Prediction in Incompressible Flow with OpenFOAM," Proceedings of the *Global Power and Propulsion Society 2023 International Technical Conference,* 2023. Paper GPPS-TC-2023-0244.	Draft paper submitted for peer review

I certify that I have obtained a written permission from the copyright owner(s) to include the above-published material(s) in my thesis. I certify that the above material describes work completed during my registration as a graduate student at the University of Windsor.

III. General

I declare that, to the best of my knowledge, my thesis does not infringe upon anyone's copyright nor violate any proprietary rights and that any ideas, techniques, quotations, or any other material from the work of other people included in my thesis, published or otherwise, are fully acknowledged in accordance with the standard referencing practices. Furthermore, to the extent that I have included copyrighted material that surpasses the bounds of fair dealing within the meaning of

the Canada Copyright Act, I certify that I have obtained a written permission from the copyright owner(s) to include such material(s) in my thesis.

I declare that this is a true copy of my thesis, including any final revisions, as approved by my thesis committee and the Graduate Studies office, and that this thesis has not been submitted for a higher degree to any other University or Institution.

ABSTRACT

This thesis applies a modified Spalart-Allmaras (SA) turbulence model, the helicity-corrected Spalart-Allmaras (HCSA) model, in incompressible steady Reynolds-averaged Navier-Stokes (RANS) computations to reduce the numerical simulation run time for fan stall inception prediction. Computations are carried out using the OpenFOAM package. This manuscript-style thesis contains two main chapters, each stemming from conference papers. First, the HCSA turbulence model is applied to a low-speed axial fan, known as the boundary layer ingestion (BLI) fan, for fan stall behavior simulation. Both RANS and unsteady RANS (URANS) with the HCSA model and RANS with the original SA model are performed, with all results compared to experimental data from the literature. The HCSA model is able to predict the stalling flow coefficient to within 0.006 of the experimentally measured value in RANS (stall margin error at 0.012), compared with a stall margin error of 0.002 in URANS. The original SA model RANS predicts stall inception very early (flow coefficient error of -0.05). The HCSA steady RANS computation is thus shown to be a good option to find the stall point at reduced computational cost. The manner in which the HCSA model steady computations identify the correct stall inception mechanism is also revealed by comparing to the URANS stall inception process. The second part of the work presents results from the original SA, HCSA and Menter shear stress transport (SST) turbulence model for a linear cascade with NACA 65-1810 blading, focusing on how and why the HCSA model is able to predict corner separations accurately. The key takeaway is that the addition to the turbulent viscosity production associated with helicity keeps the flow attached in a more realistic manner than the other turbulence models are able to achieve.

ACKNOWLEDGEMENTS

The work done in this thesis was made possible by the support of those close to me. Firstly, I am grateful for the academic guidance from my supervisor, Dr. Jeff Defoe. Because of his expertise and enthusiasm in the field of turbomachinery, I learned lots of valuable knowledge and was inspired to become an engineer. In addition, Dr. Defoe's generous time spent on reviewing my papers and thesis are gratefully acknowledged.

I would also like to acknowledge my committee members Dr. Faouzi Gherib and Dr. Nickolas Eaves for both their time in reviewing my thesis and thoughtful insight on improvements. Besides, to all Turbomachinery and Unsteady Flows Research Group members, I am grateful for your friendship and advice on my project that aided me during the past two years.

This research in my thesis was enabled in part by support provided by Compute Ontario (https://www.computeontario.ca/) and the Digital Research Alliance of Canada (https://alliancecan.ca/).

A final thank you is extended to my parents, Ming and Lin, and my fiancée, Yaqi, whose love and support have provided me with the life-changing opportunities I have been blessed with. Without your encouragement, I would not be at this point in my life. I love you!

TABLE OF CONTENTS

LIST OF FIGURES

LIST OF TABLES

CHAPTER 1
INTRODUCTION

In this thesis, the application of the Helicity-corrected Spalart-Allmaras (HCSA) turbulence model, a modification of a Reynolds-averaged Navier-Stokes (RANS) turbulence model that is based on the Spalart-Allmaras (SA) model, in fan stall inception prediction is presented; the intended application is to turbofan engines.

The turbofan is a modern variation of the basic gas turbine engine, used for aerospace propulsion. The high bypass ratio turbofan is widely used in commercial aircraft nowadays; however, because the turbofan works at different conditions, the incidence (incoming flow angle) will vary from the design value, and this can lead to flow separation in the blade passages. If the separation blocks the passage, the mass flow rate will be reduced, and thus the thrust decreases. This phenomenon is called stall. To avoid stall, the aircraft should ensure the working condition of the turbofan is within the safe working range, and this safety range is mostly currently determined by "rules of thumb" (based on the lots of experimental data) and conservative design due to the computational expense of accurately predicting stall inception using time-accurate computations. Computational fluid dynamics (CFD) is the typical way to simulate fan behavior.

Accurate axial fan/compressor stall point prediction using CFD has generally been carried out using unsteady computations, often with slowly ramped back pressure. While this approach tends to be accurate with unsteady Reynolds-averaged Navier Stokes (URANS) computations, it is computationally expensive, often requiring 4-6 rotor blade passages to be included in the computation and necessitating the solution of many rotor revolutions' worth of flow time. Recently, some work from Lopez et al. [1] has shown that the turbulence model modified by Liu et al. [2] is able, in steady RANS computations, to predict fan stall points within a few percent of experimentally measured operability limits. In this thesis, I directly predict stall points using a steady, multiple reference frame (MRF) or "frozen rotor" approach employing the HCSA turbulence model. The machine studied is a low-speed axial fan. Computations are carried out using the open-source CFD software package OpenFOAM. The approach is able to predict the stalling flow coefficient to within 0.006 of the experimentally measured value. Detailed assessments of the flow field at the

last stable operating point and a point just into stall yield show that the HCSA model, in steady computations, can predict the same stall inception mechanism captured in URANS.

In previously published work, the modified turbulence model has been implemented in in-house or commercial codes as a user add-on where the source code is unavailable. Thus, another important part of this thesis focuses on the implementation of the HCSA model in OpenFOAM. Two linear cascades, one with prescribed velocity distribution (PVD) blading and another with NACA 65-1810 blading, are used to validate the new model. The corner separation prediction improvement in the HCSA model is also analyzed by comparing the computed flow field with the original SA (both cascades) and Menter shear stress transport (SST) turbulence model (NACA cascade).

This thesis comprises two papers, which are presented as separate chapters. The first is a preliminary validation of the HCSA model in OpenFOAM for the PVD cascade, and an assessment of the fan stall point identification ability of the HCSA model in steady RANS computations for incompressible flow, and the second contains further validation on the NACA cascade and explains the fundamental reason the HCSA model is able to accurately predict corner separation behaviour.

1.1 Objectives

The thesis has the following objectives:

Objective 1. implementing the helicity-corrected Spalart-Allmaras model in OpenFOAM and verifying the separation-capturing ability of the HCSA model,

Objective 2. using the HCSA model in steady RANS to identify the fan stall point and quantifying the accuracy relative to experiment and URANS, and

Objective 3. determining how the HCSA model is able to accurately predict the stability limit of the flow in steady RANS computations for fan stall inception problems.

1.2 Overview of Contributions

The critical contributions contained in this thesis are:

1. The HCSA turbulence model is implemented successfully in OpenFOAM v2206, and this model is validated by applying it to the NACA 65-1810 cascade as well as a PVD cascade. The source code of the HCSA model is made available to all OpenFOAM users, and the implementation process is shown in Appendix A.

2. The HCSA model is shown to successfully predict a fan stall point in steady RANS computations with incompressible flow, and the stall margin error is 1.2% compared with the experiment. This shows the viability of this approach for design-stage stall margin assessment.
3. The HCSA model in steady RANS is shown to be able to capture the stall point accurately as it suppresses artificial corner separation which leads to early stall onset, and thus predicts the same stall inception mechanism as URANS.

1.3 Thesis Outline

This thesis is split into two main chapters, each primarily responsible for one of the topics mentioned. The remainder of this thesis is organized as follows. Chapter 2 details the assessment of fan stall point identification ability with the HCSA model. Chapter 3 contains the paper on implementing and verifying the HCSA model and comparing its performance to other turbulence models. Finally, Chapter 4 contains concluding remarks and recommended future work that can be performed to advance further the contributions of the HCSA model in the field of fan/compressor stall inception identification.

1.4 References

[1] D. I. Lopez, T. Ghisu, T. Kipouros, S. Shahpar, and M. Wilson, "Extending Highly Loaded Axial Fan Operability Range Through Novel Blade Design," *J. Turbomach.*, vol. 144, no. 12, Sep. 2022, doi: 10.1115/1.4055350.

[2] Y. Liu, L. Lu, L. Fang, and F. Gao, "Modification of Spalart–Allmaras model with consideration of turbulence energy backscatter using velocity helicity," *Phys. Lett. A*, vol. 375, no. 24, pp. 2377–2381, Jun. 2011, doi: 10.1016/j.physleta.2011.05.023.

CHAPTER 2
ASSESSMENT OF FAN STALL POINT IDENTIFICATION ABILITY OF STEADY RANS COMPUTATIONS WITH THE HELICITY-CORRECTED SPALART-ALLMARAS TURBULENCE MODEL

2.1 Introduction

The demand for low-cost stall prediction requires accurate computational fluid dynamics (CFD) simulations with a short run time. CFD methods for predicting multistage compressor performance have been investigated by Belamri et al.[1], who concluded that high fidelity turbulence models required refined meshing up to 2.5 million cells per passage. Typically, there are two unsteady simulation strategies that can predict stall inception. The first strategy is to increase the back pressure slowly [2], and the other is to reduce the exit area in small steps [3]. Both strategies, typically employed with unsteady Reynolds-averaged Navier-Stokes (URANS) simulations, are computationally expensive. Hewkin-Smith et al. [4] used the increasing back pressure approach and found that tip leakage flow suppresses corner separation, however, at larger tip gap sizes the increased tip leakage flow causes earlier leading edge separation. Therefore, it is clear that the crux of stall prediction is the ability to accurately capture flow separation. Steady RANS computations have generally not been regarded as being able to accurately capture flow separation behavior with standard turbulence models such as the Spalart-Allmaras (SA) model [5] or Menter's shear stress transport (SST) model [6]. Kim et al. [7] and Lee et al. [8] have verified that modified forms of the SA model, which account for local adverse pressure gradients, can predict stall shock wave boundary layer interaction correctly, and hence yield results that match experimental data well. They also carried out steady and unsteady CFD simulations of fans, and the steady simulations yield stall points to within 2.6% of flow coefficient compared with URANS and experimental data. However, the modified SA model used in Kim and Lee's research was only implemented for the compressible flow; there is no literature assessing the modified SA model's stall prediction accuracy for incompressible flows, despite there being many turbomachinery applications where Mach numbers are very low, for example ventilation fans.

Liu et al. [9] also modified the SA turbulence model with a helicity correction to account for energy backscatter; this modification affects the model performance in both

compressible and incompressible flow. They validated the modified model's ability to predict corner separation in a linear compressor cascade by comparing to experimental data, and the results indicated that the modified SA model significantly improved the ability to determine the location of flow separation. This is thus a more generally applicable modification of the SA model which does not require shock waves to be present to yield different behavior than the original SA model.

Although Liu et al. carried out RANS computations to verify the accuracy of the HCSA model compared to experimental measurements, the test was based on corner separation prediction in a linear cascade and not on fan or compressor stall prediction. The HCSA model was employed by Lopez et al. [10] to study the effect of tip leakage axial-momentum flux on design point efficiency and stability range for an axial fan. Though the HCSA stall point predictions were generally within 5% of normalized design mass flow of experimental values, there was a lack of in-depth explanation as to how the turbulence model worked since that was not the primary objective.

In this paper, we employ the HCSA model to predict fan stall using both steady and unsteady CFD simulations and compare the results to steady SA computations and experimental data. We show that the steady HCSA approach is able to predict the stalling flow coefficient to within 0.006 of the experimentally measured value. We also carried out the unsteady HCSA model to demonstrate the stall inception process and show that the steady and unsteady models are able to predict the same still inception mechanism. The original SA model predicts premature stall inception by generating a large, non-physical corner separation.

The remainder of this paper is organized as follows. In Section 2.2 we introduce the overall computational approach. Next, in Section 2.3 the fan stage studied, and numerical modeling details are presented, and then the behavior of the various numerical approaches with regards to fan stall inception is detailed in Section 2.4.

2.2 Computational Approach

Incompressible RANS and URANS flow simulations were carried out with OpenFOAM v2206, with both SA and HCSA turbulence models. Steady computations used the SimpleFOAM solver, and the unsteady computations used the PimpleFOAM solver. The implementation of the HCSA model code can be found in Appendix A. For the

fan stage studied, the multiple reference frame (MRF) strategy was utilized for the rotor region in steady computations, and a moving mesh with a sliding interface was used for the unsteady computations. Second-order accurate numerics are employed. The interfaces between rotor and stationary regions of the computational domain are handled with OpenFOAM's Arbitrary Mesh Interface (AMI) approach. The same approach is used to deal with the non-conformal mesh across the tip gap for the fan rotor.

2.3 Fan Stage Studied and Numerical Model

The test case is a low-speed axial fan, known as the boundary layer ingestion (BLI) fan, from the Whittle Lab, University of Cambridge [11].

The computational domain employed for this single-stage fan is illustrated to scale in Fig. 2.1. The main design parameters are shown in Table 2.1 and further details are provided by Gunn and Hall [12]. Perovic et al. [11] measured the time-averaged stagnation and static pressures and the swirl and radial flow angles with a five-hole pressure probe area traverse system at stations 1 and 2 in Fig. 2.1. The flow is incompressible since the highest Mach numbers are well below 0.2.

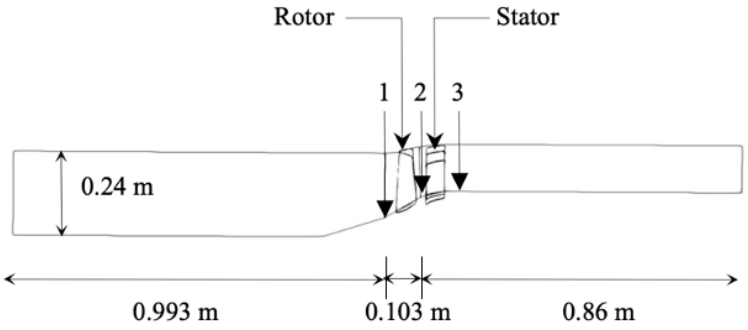

FIGURE 2.1: MERIDIONAL VIEW OF THE BLI FAN RIG COMPUTATIONAL DOMAIN

The blade geometry is approximated based on the previous work by Defoe et al. [13].

TABLE 2.1: DESIGN POINT FLOW PARAMETERS AND GEOMETRY FOR THE BLI FAN RIG

Flow coefficient $\phi = v_x/U_{mid}$	0.50
Stage loading coefficient $\psi = \Delta h_0/U_{mid}^2$	0.47
Rotor inlet tip Mach number	0.13
Rotor tip Reynolds number	200,000
Rotor speed Ω (RPM)	1800
Rotor inlet tip diameter (m)	0.48
Rotor inlet hub-to-tip radius ratio	0.3
Running tip clearance (span fraction)	0.5%
Number of rotor, stator blades	20, 30

1/10 of the annulus is modeled to obtain sectors of equal circumferential extent for both blade rows (2 rotor blades, 3 stator blades). RANS computations with the HCSA turbulence model and multiple reference frame (MRF) (often called "frozen rotor") approach are used for grid independence assessment, and both rotor and stator blade mesh were generated by ANSYS TurboGrid, using an HOH topology. The upstream region grid was generated using Pointwise with a structured hexahedral mesh, and the hub wall in the upstream region was extended to zero radius at the same slope as that in the rotor region. The downstream mesh was extended after the stator blade region in the axial direction with no change to hub or casing radius.

Figure 2.2 depicts the surface grid at the leading edge tip of the rotor blade (a); the mesh on the rotor hub is also shown (b). The tip gap for the rotor is 0.5% of span, and the target y^+ was 3 on all solid walls.

To ensure grid independence, four grids were generated, with approximately 0.5 million, 1 million, 2 million and 2.5 million cells for each blade passage. The design point flow field was determined for these grids. The stage pressure rises coefficients obtained are 0.874, 0.858, 0.847 and 0.844, respectively. The 2 million grid per passage level is used for the stage stall assessment as the pressure rise obtained is less than 0.5% different than that obtained on the finer grid. The total number of cells for the domain that includes the upstream duct, 2 rotor blade passages, 3 stator blade passages, and a downstream duct region is 12.4 million.

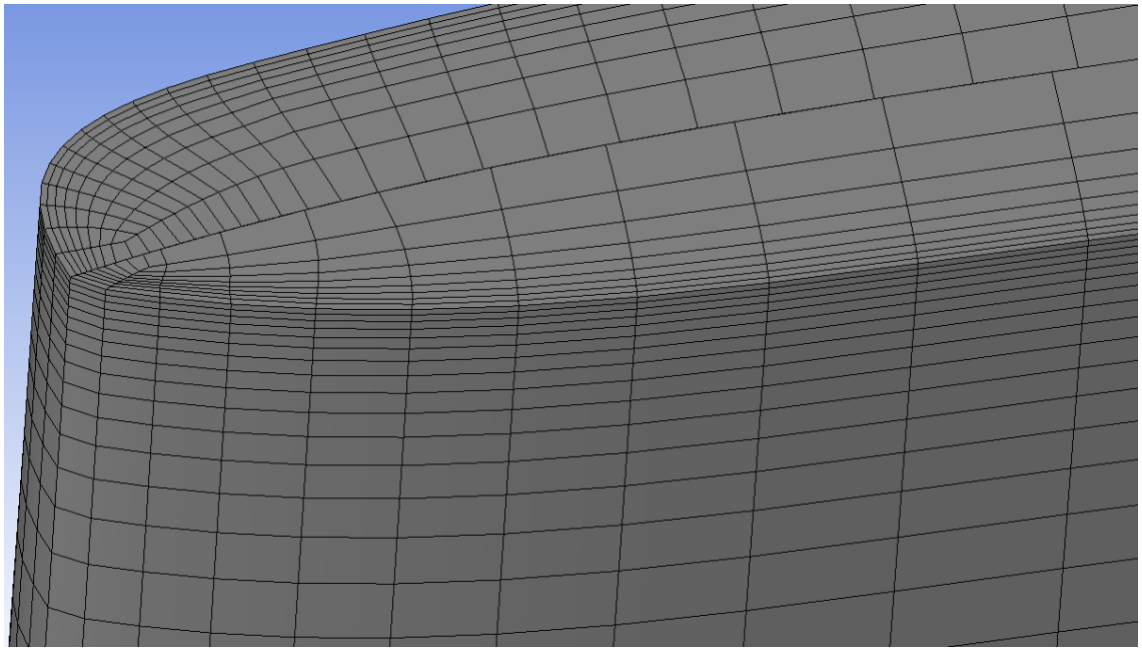

(a) Leading edge grid

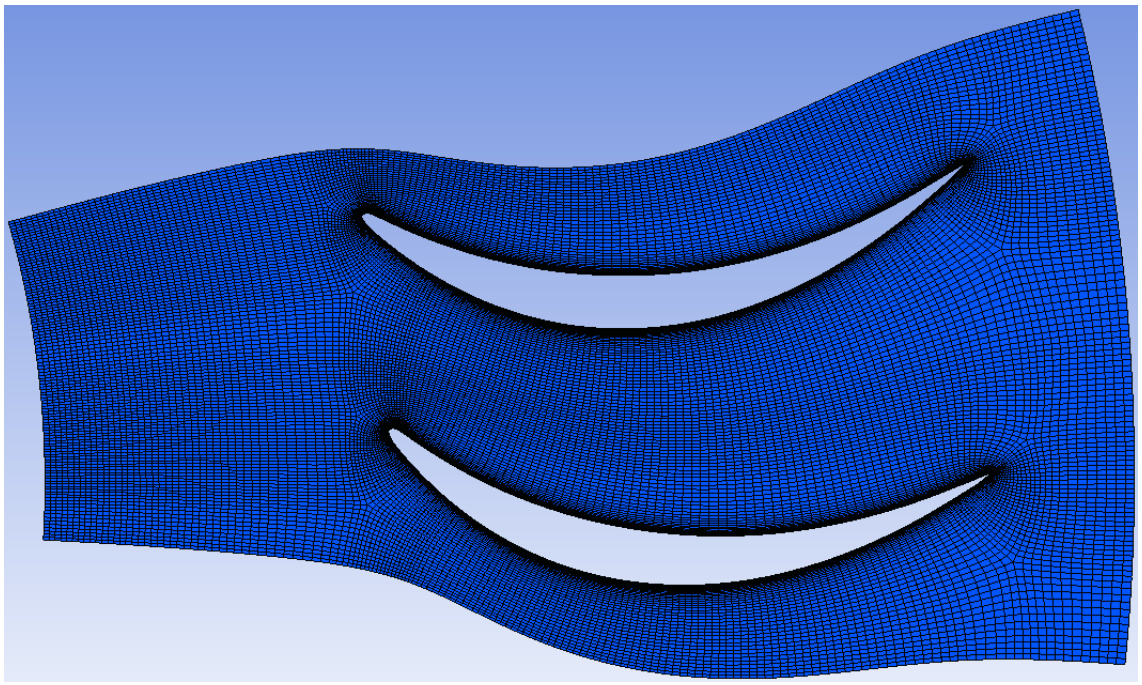

(b) Rotor hub grid

FIGURE 2.2: GRID GENERATION OF (A) LEADING EDGE OF ROTOR BLADE AND (B) THE HUB MESH OF ROTOR BLADE.

The inlet boundary conditions required specification of four parameters (or their gradients): the modified turbulent viscosity $\tilde{\nu}$, the molecular kinematic viscosity ν [1], pressure p, and velocity v. The molecular kinematic viscosity is constant (air at standard conditions). In this fan case, the molecular kinematic viscosity [2] at inlet is 20% of the modified turbulent viscosity, and the modified turbulent viscosity $\tilde{\nu}$ is:

$$\tilde{\nu} = \sqrt{\frac{3}{2}}(v_1 I l) \quad (2.1),$$

where, v_1 is the inlet mean flow velocity, I is the turbulence intensity (1%) and l is the turbulent length scale (1% of inlet radius).

At the design point, the inlet pressure boundary condition is zero gradient, and the flow coefficient was controlled by setting the inlet flow velocity. For the steady computations, the other operating points were initialized from the results of the first simulation. The inlet total pressure is held constant using the value determined from the design point (with the velocity gradient set to zero at the inlet), and varying outlet static pressure is used to move to different flow coefficients. The first point at which the simulation fails to converge is deemed to be in stall. We also carried out the same computations with the standard SA model to assess the impact of the modified turbulence model.

The unsteady computation is initialized from the steady case. The initial total pressure at inlet and outlet, as well as the internal field were kept from the steady case with the flow coefficient at 0.449. The unsteady case used a rotating mesh for the rotor instead of the MRF approach, and there were 300 physical time steps per rotor blade pitch passing period. The flow coefficient was decreased by 0.0013 per rotor revolution by raising the outlet static pressure slowly. The unsteady computations use the same 1/10th annulus domain as the steady computations.

The convergence criteria are based on normalized residual reduction to 0.0002 for all governing equations. The relaxation factor for all equations was 0.3.

2.4 Results and Discussion

For the steady RANS computations, 10 operating points are computed to predict the stall point. For the HCSA model, nine simulations at flow coefficients from 0.437 to

1. The molecular kinematic viscosity is a typographical error in the published paper. Right here should be the kinematic turbulent viscosity.
2. The same typographical error as 1 and the accurate description can be found on page 24.

0.531 converged, while when the flow coefficient dropped to just above 0.43, convergence could no longer be achieved.

The SA model simulations were started from the flow coefficient at 0.505, and the last stable point is at 0.478.

The URANS with HCSA finished running within approximately one month using 108 cores; in contrast, the average run time for each convergent operating point with the steady approach was around 20 hours with 108 cores.

Figure 2.3 shows the measured clean flow characteristic (from Ref. [12]) and the computed results. The stage pressure rise coefficient φ and flow coefficient ϕ are:

$$\varphi = \frac{p_{03} - p_{01}}{0.5\rho U_{mid}^2} \quad (2.2),$$

$$\phi = \frac{v_x}{U_{mid}} \quad (2.3).$$

All data is mass-averaged.

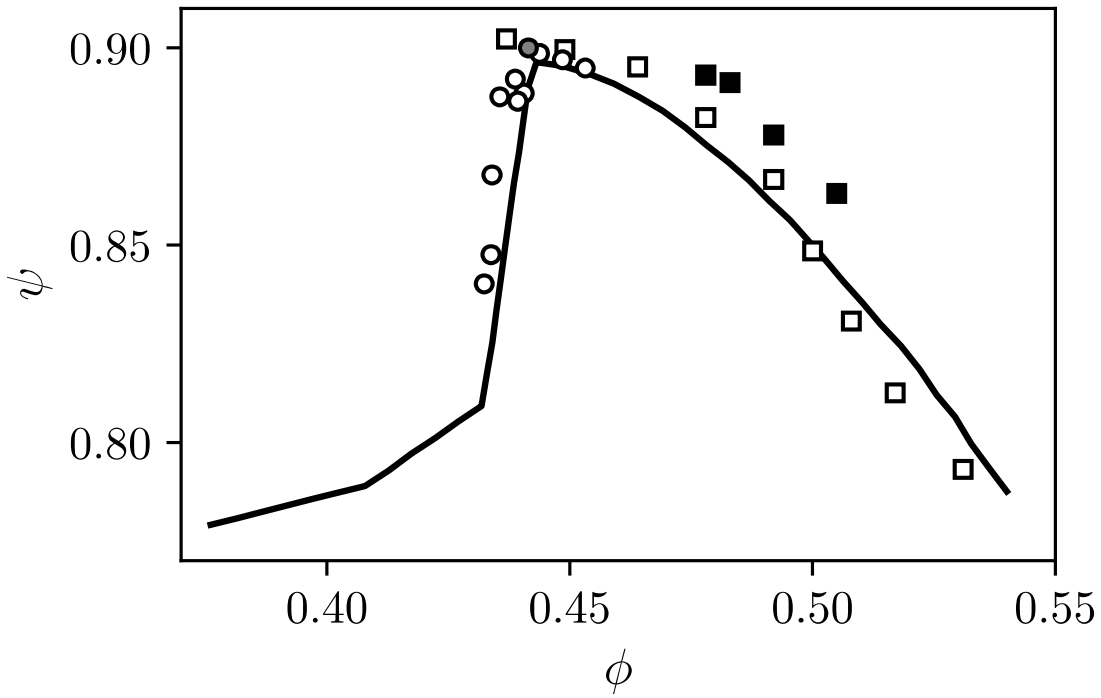

FIGURE 2.3: EXPERIMENTALLY MEASURED AND COMPUTED CLEAN FLOW CHARACTERISTIC FOR THE BLI FAN. SOLID LINE: MEASUREMENTS [13]; OPEN SQUARES: STEADY HCSA; FILLED SQUARES; STEADY SA; OPEN CIRCLES: UNSTEADY HCSA; GREY CIRCLE: LAST STABLE OPERATING POINT FOR UNSTEADY HCSA.

The flow coefficient of 0.437 is the last stable operating point for the steady HCSA model. When the outlet pressure dropped slightly, the HCSA model failed to converge, indicating stall. The predicted stalling flow coefficient is within 0.006 of the measured value, yielding a stall margin of 0.126, compared to the measured value of 0.114. The stall margin is

$$SM = \frac{\phi_{design} - \phi_{laststable}}{\phi_{design}} \quad (2.4).$$

So, the HCSA model in steady RANS is able to predict the stall margin to within 0.012. Away from stall, the RANS approach is also able to accurately predict the stage pressure rise characteristic with an RMS error of 0.2%, though the slope is slightly steeper. Note that design-point performance is extremely well-predicted (0.849 compared to 0.847 measured).

The last stable point for the unsteady computations is at ϕ=0.442, yielding a stall margin of 0.116, which is 0.002 larger than the experimentally measured value; they are nearly identical. When the flow coefficient drops below 0.442, the flow coefficient and pressure rise coefficient fluctuate as stall inception occurs, shown in Fig 2.4. τ_{rev} is the period for one full revolution for the rotor. The onset of instability is clear as the point where pressure rise decreases with decreasing flow coefficient. As expected, the pressure rise drops dramatically over a very small change in ϕ.

However, the steady SA model predicts a stall point far away from the measured one. The subsequent discussion will highlight differences in the flow fields between the HCSA and SA model solutions. Table 2.2 collects the last stable operating point and stall margin information for the data shown in Fig. 2.5. The three key takeaways are that (1) the URANS captures the measured SM very accurately, (2) the HCSA model reduces the error in stall margin for steady RANS by a factor of 4, and (3) the HCSA model in RANS is the only computational approach which yields stable operating points at flow coefficients appreciably below the measured stall point.

TABLE 2.2: COMPARISON OF LAST STABLE OPERATING POINTS AND STALL MARGIN

Method	Last Stable ϕ	SM	SM error
Experiments [12]	0.443	0.114	-
URANS, HCSA	0.442	0.116	0.002
RANS, HCSA	0.437	0.126	0.012
RANS, SA	0.478	0.064	-0.05

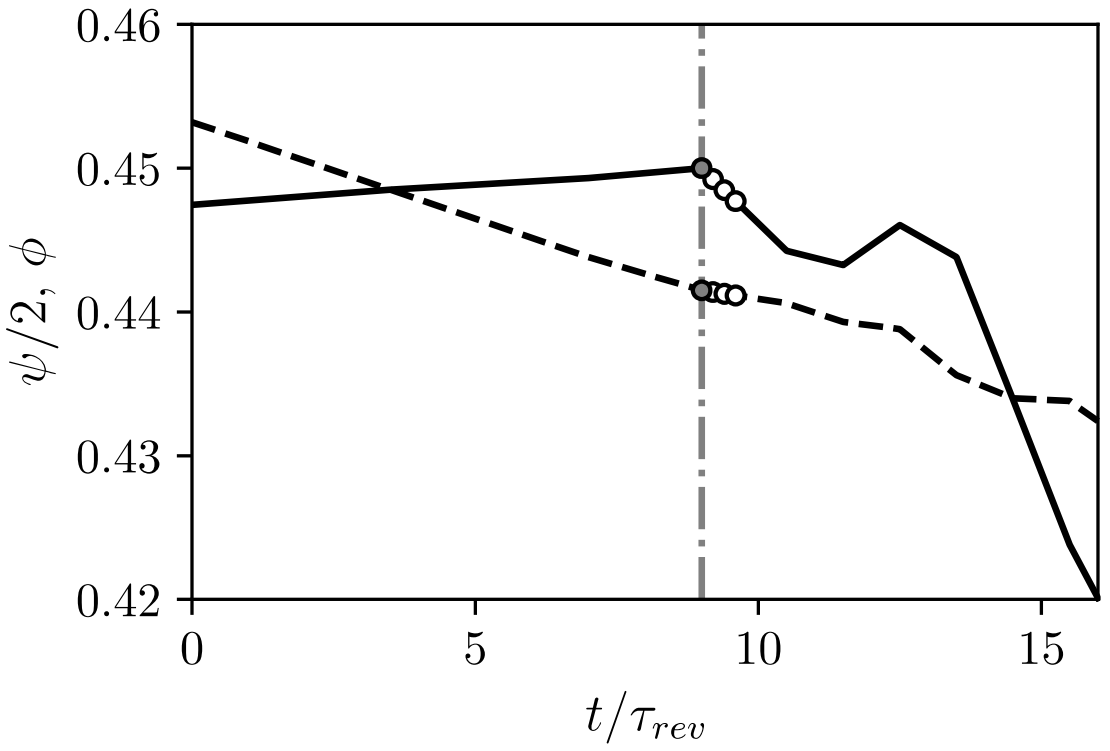

FIGURE 2.4: FLOW COEFFICIENT AND (HALVED) STAGE PRESSURE RISE COEFFICIENT VS. TIME IN ROTOR REVOLUTIONS FOR STALL INCEPTION IN UNSTEADY HCSA COMPUTATION. SOLID LINE: STAGE PRESSURE RISE COEFFICIENT; DASHED LINE: FLOW COEFFICIENT. GRAY CIRCLES AND VERTICAL LINE: LAST STABLE OPERATING POINT; WHITE CIRCLES: OPERATING POINTS SHOWN IN FIG. 2.5(d)

Figure 2.5 shows the radial vorticity for the steady HCSA, steady SA, and unsteady HCSA computations at 95% span. The normalized radial vorticity is defined as:

$$\widetilde{\omega}_r = \frac{\omega_r}{\Omega} \tag{2.5}.$$

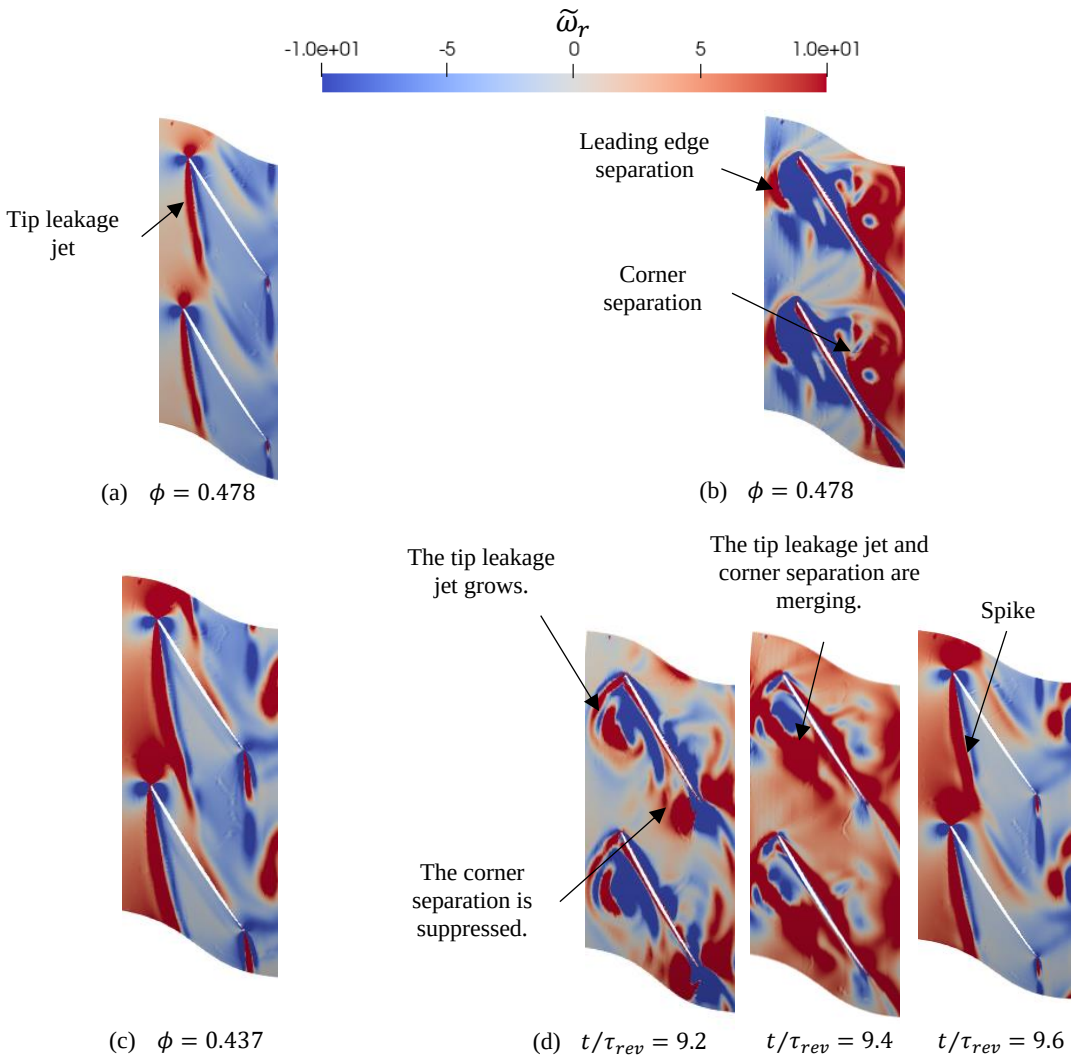

FIGURE 2.5: CFD COMPUTED NORMALIZED RADIAL VORTICITY IN THE ROTOR AT 95% SPAN. (A) STEADY HCSA, $\boldsymbol{\phi = 0.478}$; (B) STEADY SA, $\boldsymbol{\phi = 0.478}$ (LAST STABLE POINT); (C) STEADY HCSA, $\boldsymbol{\phi = 0.437}$ (LAST STABLE POINT); AND (D) STALL INCEPTION PROCESS (UNSTEADY HCSA)

For the last stable point predicted by the SA model (ϕ=0.478), Fig. 2.5(a) shows that the tip leakage jet is nearly tangential in the steady HCSA computation, and the influence of corner separation is small. However, for the SA model in Fig. 2.5(b), the effect of corner separation is overestimated, and the tip leakage separation is affected by the corner separation. The operating condition is marginally stable and any further decrease in flow coefficient will result in stall. In the steady computations using the SA model, the dominant reason for (premature) stall is the growth of the corner separation.

Figure 2.5(c) shows that when the operating point is close to the stall point, the HCSA model still predicts no dominant corner separation, while the tip leakage flow gives rise to leading edge separation, and finally causes stall inception. The stall inception process in the unsteady computation is shown in Fig. 2.5(d). Initially ($t/\tau_{rev} = 9.2$) the corner separation is suppressed by the tip leakage separation, then ($t/\tau_{rev} = 9.4$) the growth of the tip leakage flow causes these two separations to merge. Because of this large separation near the leading edge, the rotor passages are blocked ($t/\tau_{rev} = 9.6$), and hence causes a sharp decline of pressure rise.

Comparing Fig. 2.5(c) and the final image in Fig. 2.5(d), it is clear that the HCSA model is finding a solution which looks almost identical to the going-into-stall flow field from the unsteady computation, which explains why the last stable flow coefficient with the HCSA model is lower than the actual stall point.

2.5 Conclusions

In this paper, it has been shown that steady RANS with the HCSA model is able to more accurately predict the flow field around the stall point for a low-speed fan by essentially eliminating non-physical large corner separations that the original SA model produces. The improved ability of the HCSA model to determine when flow stays attached on highly-loaded compressor blades means that steady computations are able to predict the same stall inception mechanism as unsteady computations (in this case, passage blockage at the leading edge due to the tip leakage jet causing separation on the blade leading edge). This means that, referring back to Table 2.2, the steady simulation with the HCSA model can predict the stall margin to within 0.01 while reducing the computational cost by roughly an order of magnitude compared to URANS. It is also important to note that the steady HCSA computations can over-predict the stall margin, so some caution is required in their use.

This paper contributes to the body of knowledge suggesting the HCSA turbulence model makes steady RANS computations useful for stall prediction in axial turbomachines and shows that the approach is just as useful in incompressible flows as in the compressible flows previously presented in the literature.

2.6 Nomenclature

Symbols

p	Pressure
U	Blade speed
v	Velocity
ρ	Density
ϕ	Flow coefficient
φ	Stage total-to-total pressure rise
τ_{rev}	Time period for one revolution
ω	Vorticity
$\widetilde{\omega}$	Normalized vorticity
Ω	Rotor speed

Subscripts

0	Stagnation quantity
1	Station number (rotor inlet)
2	Station number (rotor outlet and stator inlet)
3	Station number (stator outlet)
R	Radial
x	Axial
tip	Blade tip
mid	Mid-span
rev	Rotor revolution
LE	Leading edge
TE	Trailing edge
PS	Pressure surface
SS	Suction surface

2.7 References

[1] T. Belamri, P. Galpin, A. Braune, and C. Cornelius, "CFD Analysis of a 15 Stage Axial Compressor: Part I — Methods," presented at the ASME Turbo Expo 2005: Power for Land, Sea, and Air, American Society of Mechanical Engineers Digital Collection, Nov. 2008, pp. 1001–1008. doi: 10.1115/GT2005-68261.

[2] R. Mito and S. Yamashita, "Prediction of Rotating Stall During Startup for Axial Compressors," presented at the ASME Turbo Expo 2019: Turbomachinery Technical Conference and Exposition, American Society of Mechanical Engineers Digital Collection, Nov. 2019. doi: 10.1115/GT2019-91340.

[3] R. H. Sundararaj, T. C. Sekar, R. Arora, and A. Kushari, "Effect of nozzle exit area on the performance of a turbojet engine," *Aerosp. Sci. Technol.*, vol. 116, p. 106844, Sep. 2021, doi: 10.1016/j.ast.2021.106844.

[4] M. Hewkin-Smith, G. Pullan, S. D. Grimshaw, E. M. Greitzer, and Z. S. Spakovszky, "The Role of Tip Leakage Flow in Spike-Type Rotating Stall Inception," *J. Turbomach.*, vol. 141, no. 6, Jun. 2019, doi: 10.1115/1.4042250.

[5] P. Spalart and S. Allmaras, "A one-equation turbulence model for aerodynamic flows," in *30th Aerospace Sciences Meeting and Exhibit*, in Aerospace Sciences Meetings. American Institute of Aeronautics and Astronautics, 1992. doi: 10.2514/6.1992-439.

[6] F. R. Menter, "Two-equation eddy-viscosity turbulence models for engineering applications," *AIAA J.*, vol. 32, no. 8, pp. 1598–1605, Aug. 1994, doi: 10.2514/3.12149.

[7] S. Kim, G. Pullan, C. A. Hall, R. P. Grewe, M. J. Wilson, and E. Gunn, "Stall Inception in Low-Pressure Ratio Fans," *J. Turbomach.*, vol. 141, no. 7, Feb. 2019, doi: 10.1115/1.4042731.

[8] K.-B. Lee, M. Wilson, and M. Vahdati, "Validation of a Numerical Model for Predicting Stalled Flows in a Low-Speed Fan—Part I: Modification of Spalart–Allmaras Turbulence Model," *J. Turbomach.*, vol. 140, no. 5, Apr. 2018, doi: 10.1115/1.4039051.

[9] Y. Liu, L. Lu, L. Fang, and F. Gao, "Modification of Spalart–Allmaras model with consideration of turbulence energy backscatter using velocity helicity," *Phys. Lett. A*, vol. 375, no. 24, pp. 2377–2381, Jun. 2011, doi: 10.1016/j.physleta.2011.05.023.

[10] D. I. Lopez, T. Ghisu, T. Kipouros, S. Shahpar, and M. Wilson, "Extending Highly Loaded Axial Fan Operability Range Through Novel Blade Design," *J. Turbomach.*, vol. 144, no. 12, Sep. 2022, doi: 10.1115/1.4055350.

[11] D. Perovic, C. A. Hall, and E. J. Gunn, "Stall Inception in a Boundary Layer Ingesting Fan," *J. Turbomach.*, vol. 141, no. 9, Jun. 2019, doi: 10.1115/1.4043644.

[12] E. J. Gunn and C. A. Hall, "Aerodynamics of Boundary Layer Ingesting Fans," presented at the ASME Turbo Expo 2014: Turbine Technical Conference and Exposition, American Society of Mechanical Engineers Digital Collection, Sep. 2014. doi: 10.1115/GT2014-26142.

[13] J. Defoe, Q. Minaker, and W. Altenhof, "Estimation of Unsteady Blade Loading Due to Inlet Distortion Using a Body Force Rotor Model," presented at the the 15th International Symposium on Unsteady Aerodynamics, Aeroacoustics & Aeroelasticity of Turbomachines, Sep. 2018. doi: ISUAAAT15-084.

CHAPTER 3
VALIDATION OF HELICITY-CORRECTED SPALART-ALLMARAS MODEL FOR CORNER SEPARATION PREDICTION IN INCOMPRESSIBLE FLOW WITH OPENFOAM

3.1 Introduction

Three-dimensional computational fluids dynamics (CFD) is critical to compressor and fan stage blade design and assessment, and for accurate determination of stall margin, most commonly unsteady Reynolds-averaged Navier-Stokes (URANS) computations are used. In the industrial design cycle, though, URANS can still be prohibitively expensive. There is thus a strong motivation to gain confidence in turbulence modelling approaches which enable accurate stall point determination with steady RANS. This requires accurate determination of the onset of flow separations. In particular, it is critical that corner separations are accurately captured.

Menter's shear stress transport (SST) model [1], the Spalart-Allmaras (SA) model [2] and modifications of these are widely used in turbomachinery. The SST model has proved to accurately predict secondary flows near corners in RANS [3]. Yin et al. [4] carried out computations for an axial compressor using both the SST and SA models. They compared the compressor's mass flow rate at choke for the design speed, and it was found that the SST model matched the experimental data to within 0.344% while the SA model over-predicted the choking mass flow rate by 6.6%. Notably, although the computed results with the SST model were accurate overall, the tip clearance/shock interaction loss was underestimated, so there is room for improvement.

To predict compressor and fan behaviour more accurately, Lee et al. [5] employed a modified SA model that includes the effects of adverse pressure gradients. This modified SA model increased the turbulent viscosity in the region of shock wave boundary layer interaction, which directly improved the accuracy of separation point prediction and consequently showed the CFD choking mass flow at 100% speed was only 0.6% above the measured value. Kim et al. [6] investigated rotating stall by adopting the modified SA model from Lee et al., and they found that the modified SA model predicted the stall inception mechanism to be consistent with the experimental data. Notably, both RANS and

URANS computations with the modified SA model were conducted in Kim et al.'s work, and RANS was able to accurately predict the fan performance characteristic, in line with URANS and experiments. Both works showed that it was possible to accurately predict the stall point at low computational cost by using the modified SA model in compressible flow. However, since their modifications focused on capturing shock-boundary layer interactions, for lower Mach number flows without strong shocks it is not clear if their modified model is adequate. A different modified form of the SA model was proposed and validated by Liu et al. [7] and was originally assessed for incompressible flow, and in a linear cascade was shown to predict the corner separation much more accurately than the original SA model. This approach is known as the helicity-corrected SA (HCSA) model. Lopez et al. [8] performed steady compressible flow simulations using the HCSA model to reveal the effect of tip leakage axial-momentum flux on design point efficiency and stability range for an axial fan, and they were able to predict stalling mass flows to within 0.81% and 3.8% of experimental data for a reference design at 103% and 95% speeds, respectively. Yu et al. [9] [1] implemented the HCSA model in OpenFOAM v2206 [10] and applied it to stall prediction for a single-stage axial fan with incompressible flow, finding that the stall margins predicted with the HCSA model in steady RANS and URANS were predicted to within 1.2% and 0.2% of design flow coefficient, respectively.

The backward energy transport, termed energy backscatter by Leith [11], exists in all kinds of turbulence. In the theory of Lesieur [12], energy backscatter is evident in regions with coherent structures like mixing layers and rotating turbulence. A lack of backscatter can lead to inaccurate flow field predictions for the internal flow in compressor and fan blade passages. Liu et al. [7] found that the helicity is able to represent the energy backscatter, and so they modified the SA model by introducing the helicity into the production term of the SA variable transport equation. They assessed the modified model's ability to predict corner separation in a linear compressor cascade by comparison to experimental data, showing that the HCSA model accurately determined the location and size of the corner separation.

The SA model is a one-equation [2] model that solves the transport equation for the modified kinematic turbulence viscosity $\tilde{\nu}$, and the kinematic turbulence viscosity ν_t is calculated by

1. Reference 9 is presented in Chapter 2 as a published paper.

$$\nu_t = \tilde{\nu} f_{v1} \tag{3.1},$$

where the function f_{v1} is

$$f_{v1} = \frac{\chi^3}{\chi^3 + C_{v1}^3}. \tag{3.2},$$

In equation 2, the constant $C_{v1} = 7.1$ and

$$\chi = \frac{\tilde{\nu}}{\nu} \tag{3.3},$$

where ν is the molecular kinematic viscosity.

The transport equation for $\tilde{\nu}$ in the original SA is

$$\frac{D(\rho\tilde{\nu})}{Dt} = \underbrace{C_{b1}\rho\tilde{S}\tilde{\nu}}_{(Production)} - \underbrace{C_{w1}\rho f_w \left(\frac{\tilde{\nu}}{d}\right)^2}_{(Dissipation)} + \underbrace{\frac{1}{\sigma_{\tilde{\nu}}}\left\{\frac{\partial\left[(\mu+\rho\tilde{\nu})\frac{\partial\tilde{\nu}}{\partial x_j}\right]}{\partial x_j} + C_{b2}\rho\left(\frac{\partial\tilde{\nu}}{\partial x_j}\right)^2\right\}}_{(Diffusion)} \tag{3.4},$$

where D/D_t denotes the substantial derivative and

$$f_w = g\left[\frac{(1+C_{w3}^6)}{(g^6+C_{w3}^6)}\right]^{\frac{1}{6}} \tag{3.5},$$

$$g = r + C_{w2}(r^6 - r) \tag{3.6},$$

$$r = \frac{\tilde{S}}{\tilde{S}\kappa^2 d^2} \tag{3.7},$$

$$\tilde{S} = \varpi + \frac{\tilde{\nu}}{\kappa^2 d^2} f_{v2} \tag{3.8},$$

$$f_{v2} = 1 - \frac{\chi}{1+\chi f_{v1}} \tag{3.9}.$$

In equations 4-9, ϖ is the vorticity, ρ is the fluid density, d is the distance from the wall, and C_{b1}, C_{b2}, C_{w1}, C_{w2}, C_{w3}, $\sigma_{\tilde{\nu}}$, and κ are constants whose values can all be found in Spalart and Allmaras' original paper [2].

In the HCSA model, the coefficient of the vorticity term in $\tilde{S}$ (equation 8) is modified to depend on the normalized helicity. The modified $\tilde{S}_{MSA}$, which replaces $\tilde{S}$, is

$$\tilde{S}_{MSA} = \underbrace{\left(1 + C_{h_1} h^{C_{h_2}}\right)}_{Corrected\ Helicity} \varpi + \frac{\tilde{\nu}}{\kappa^2 d^2} f_{v2} \tag{3.10},$$

where C_{h_1} is 0.71 and C_{h_2} is 0.6, according to Liu's numerical tests. The normalized helicity h is

$$h = \frac{|v \cdot \varpi|}{\|v\|\|\varpi\|} \tag{3.11},$$

where v is the velocity.

The HCSA model computation in Liu's research was carried out in Ansys FLUENT [13] and the implementation's source code is not available. In addition, the linear cascade used as a validation case by Liu et al. is based on geometry that is not publicly available.

The aims of this paper are to (1) demonstrate the implementation of the HCSA model in an open-source code, and (2) gain insight into the underlying differences between the SA, HCSA, and SST turbulence models which cause differences in predicted flow separation behaviour in compressor blade passages. Since Liu et al. [7] implemented the HCSA model and tested its ability of flow separation predicting on a linear Prescribed Velocity Distribution (PVD) cascade, in this paper, we instead work with a NACA 65-1810 linear cascade. Steady-state incompressible flow simulations for the SA, HCSA, and SST models are carried out to compare the accuracy of flow separation prediction relative to experimental data, and to gain insight into how the manner in which the turbulence models are formulated affects that accuracy.

The remainder of this paper is organized as follows. First, we introduce the linear cascade used as a test case. In the methodology section, the grid details, and the computational approach with OpenFOAM is introduced. The results and discussion section focuses on the comparison of the three different turbulence models with experimental results, as well as analysis to explain the improvements seen with the HCSA model.

3.2 Test Case

The case studied is from Kang and Hirsch's [14] experiment. They investigated a low-speed linear compressor cascade in a blower-style configuration wind tunnel. The inflow passes through a row of guide vanes, a diffuser, a setting chamber, and a nozzle before reaching the test section. The test section consists of 7 blades, installed between two parallel plates which were aligned horizontally. A 3 cm gap is introduced between the two extreme blades and the nozzle side wall to remove the side wall boundary layers. There are two variable flaps placed at the exit of the two extreme blades to maximize the periodicity for the central blades.

3.2.1 Cascade Geometry

The cascade uses NACA 65-1810 blading, and Table 3.1 shows the detailed blade parameters.

TABLE 3.1: NACA 65-1810 BLADE PARAMETER

Chord length (cm)	20
Aspect ratio	1
Solidity	1.111
Stagger angle	10°
Blade inlet angle	32.5°
Blade outlet angle	-12.5°
Design inlet flow angle	30°
Design incidence	-2.5°
Leading edge radius (cm)	0.1374
Trailing edge radius (cm)	0.2

3.2.2 Experimental Measurements

Five-hole probes installed at planes ahead of, within, and downstream of the cascade are used to measure the time-averaged flow field via traverses. The details of the measurements are described in Kang's report [15]. Table 3.2 shows the inlet flow conditions at 40% chord upstream of the cascade blade leading edge in the experiment.

TABLE 3. 2: EXPERIMENTAL INLET FLOW CONDITIONS

Constant inlet velocity (m/s)	23.7
Reynolds number based on the inlet velocity and blade chord	290,000
Free stream turbulence intensity	3.4%
Endwall boundary layer shape factor	1.22
Endwall boundary layer displacement thickness (cm)	0.14
Endwall boundary layer thickness (cm)	5

3.3 Methodology

In this section, we introduce the computational details used in this paper for studying the turbulence models.

3.3.1 Grid Generation

AutoCAD version 2023 [16] is used to generate the cascade blade geometry from the NACA 65-1810 blade coordinates in [14]. The computational domain, spanning a single blade passage, is generated using the OpenFOAM tools blockMesh and snappyHexMesh. The domain and outer boundaries are initially created without the blade present by using blockMesh, and then the blade shape is subtracted, and the surrounding grid refined using snappyHexMesh. Boundary layers cells are added on the blade surface by snappyHexMesh and the OpenFOAM tool refineWallLayer is used successively to create the endwall boundary layer cells. Figure 1 (a) shows the blade-to-blade view of the cascade mesh. The inlet and outlet boundaries are located 40% and 150% of the blade chord away from the blade leading and trailing edges, respectively. The inlet is close to the leading edge, but this location is used since the inlet conditions (including endwall boundary layer details) are specified in Kang and Hirsch's work [14] at this location. The computational domain covers half the span, with a symmetry plane specified at mid-span, since the inlet condition is symmetric, and Kang and Hirsch's results focus on the flow details near the upper endwall. Cyclic (periodic) boundary conditions are used to enable use of a single passage domain. 17 boundary layer cells are used with a first cell target y^+ of 3 on both the endwall and blade surfaces. Figure 1 (b) shows both boundary layer grids where the endwall and blade suction surface meet.

The overall cell count is approximately 2.9 million cells. To establish grid independence, grids with 0.6 million, 1 million, 1.64 million, and 3.3 million cells were also assessed. The mass-averaged total pressure loss between the inlet and outlet increased by 1.18% between the 2.9 million and 3.3 million cell grids. Compared with the averaged total pressure loss change at 12% among the 0.6 million, 1 million, and 1.64 million grids, the 2.9 million cell grid was suitable for all computations in this paper.

3.3.2 Computational Approach

All the CFD simulations that are carried out are incompressible, steady RANS computations using the SimpleFOAM solver from OpenFOAM v2206 with the HCSA, original SA, and k-ω SST turbulence models. The HCSA implementation into OpenFOAM v2206 is detailed in Yu et al. [9]. Convergence criteria for all three models are identical,

with normalized residual decreases by three orders of magnitude. The maximum y^+ across all models is approximately 2.5 and the average y^+ is at the highest 0.64.

The velocity and pressure boundary conditions are the same for all three models. Conditions are set to match those measured experimentally: the inlet velocity v_1 is 23.7 m/s at 30°, and all the inlet pressure boundary condition is zero gradient. For the SA and HCSA models, the inlet kinematic turbulent viscosity ν_t is 20% of the inlet modified turbulence viscosity $\tilde{\nu}$, and the inlet modified turbulent viscosity $\tilde{\nu}$ is

$$\tilde{\nu} = \sqrt{\frac{3}{2}}(v_1 I l) \tag{3.12},$$

where l is the turbulent length scale (0.011 m, 22% of the boundary layer thickness [17]). For the k-ω SST turbulence model, the inlet turbulence kinetic energy k is

$$k = \frac{3}{2}(v_1 I)^2 \tag{3.13},$$

and the specific turbulent dissipation rate ω is

$$\omega = 0.09^{-0.25}\frac{\sqrt{k}}{l} \tag{3.14}.$$

The outlet static pressure is imposed to be uniform in all computations, and the outlet velocity gradient is set to zero.

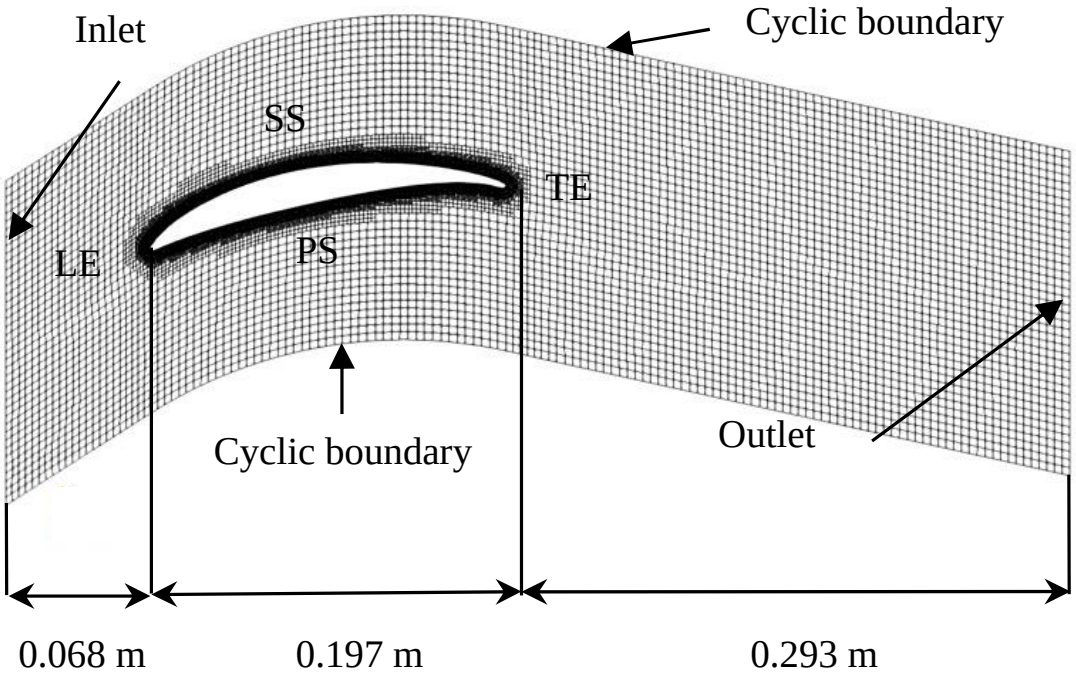

(a)

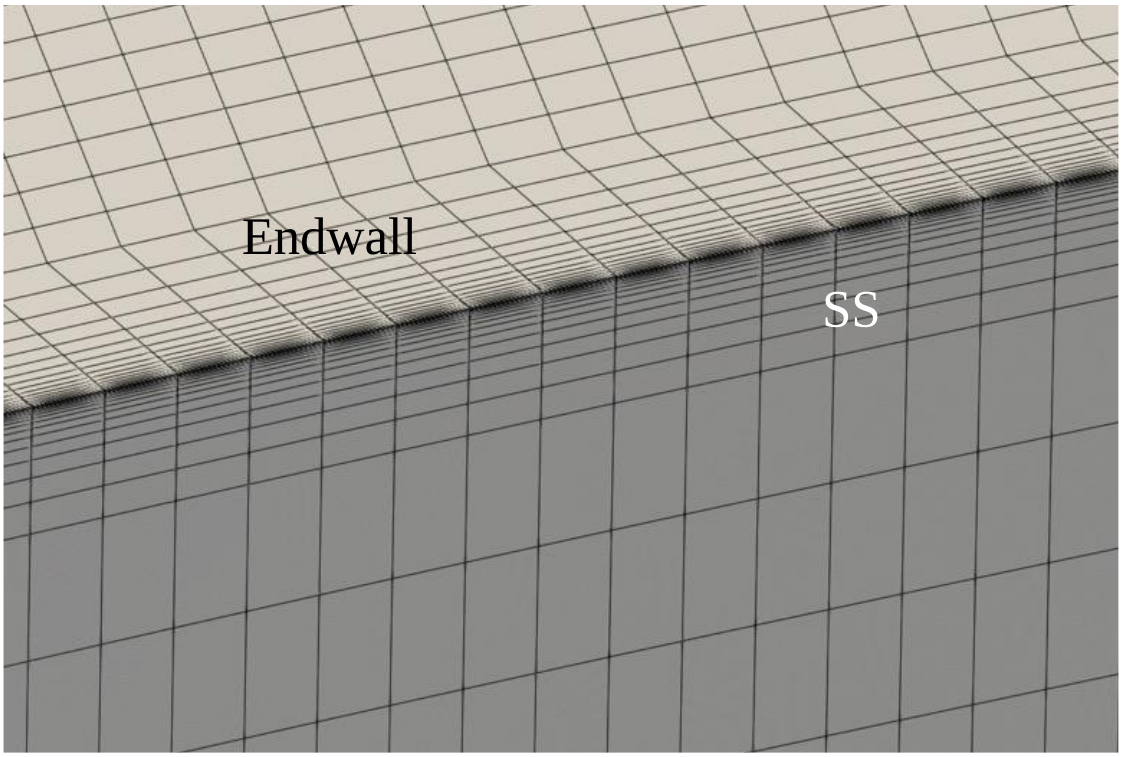

(b)

FIGURE 3.1: LINEAR CASCADE MESH: (A) BLADE-TO-BLADE VIEW AND (B) DETAIL OF THE BOUNDARY LAYER CELLS WHERE THE ENDWALL AND BLADE SUCTION SURFACE MEET.

3.4 Results and Discussion

All computations are performed at the design incidence (-2.5°). The computed and experimental blade surface static pressure coefficient C_p distributions at 99%, 98.5%, and 50% span are shown in Figure 3.3. C_p is defined as:

$$C_p = \frac{p - p_1}{\frac{1}{2}\rho {v_1}^2} \quad (15),$$

where p_1 and p are the inlet and local static pressures, respectively.

From Fig. 3.2, the HCSA model accurately predicts the blade loading across the span. At 98.5% and especially at 99% span, the corner separation size is over-estimated by the SA and SST models, but the HCSA correctly predicts that the flow remains attached on the pressure surface. This improvement in the ability to capture corner separation when it physically occurs, but not to predict that it will occur when it should not, seems to be the

cornerstone of the HCSA model's benefit. This result validates the HCSA model implementation in OpenFOAM.

Turning attention to the 50% span results, the SST model is able to accurately capture the loading, as the lower loading towards the trailing edge here compared to near the endwall does not lead to over-prediction of separation. Even at midspan, the original SA model struggles to get the loading right at the trailing edge, especially on the pressure surface.

To link the changes in loading predicted by the various models to changes in loss, in Fig. 3.3 we show the loss coefficient across the passage 25% chord downstream of the trailing edge. The total pressure loss coefficient Y_p is defined as

$$Y_p = \frac{p_{01} - p_{02}}{\frac{1}{2}\rho {v_1}^2} \tag{3.16},$$

where p_{01} is the inlet total pressure and p_{02} is the local total pressure on a plane 25% chord downstream of the trailing edge.

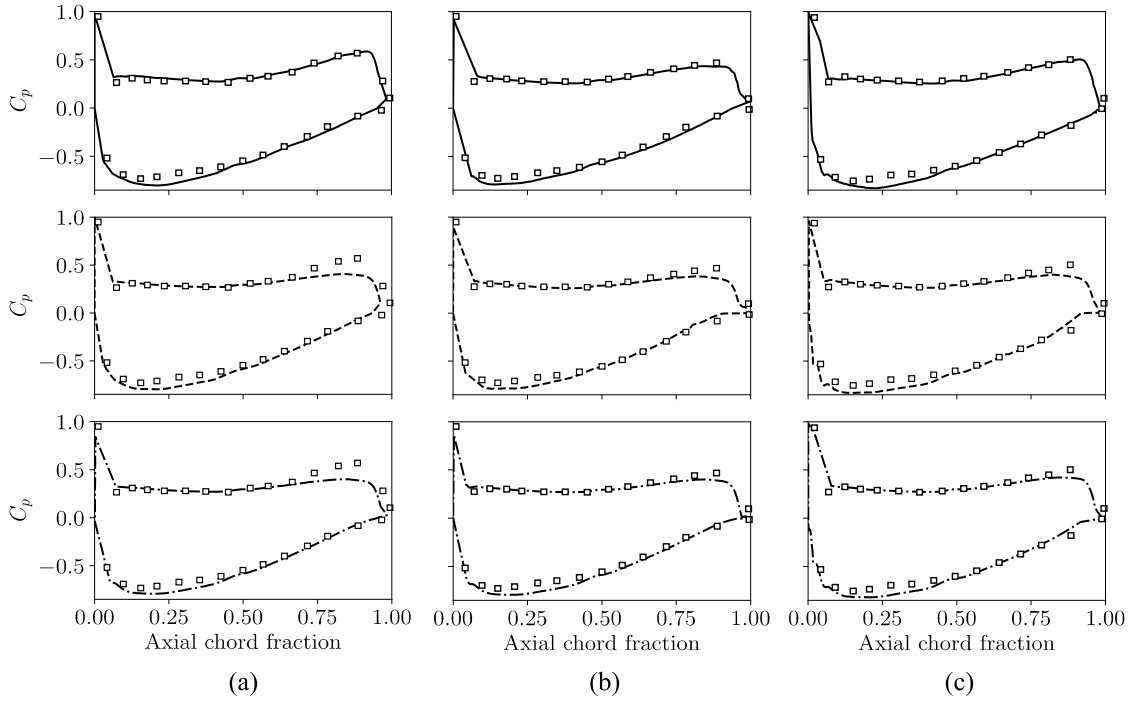

FIGURE 3.2: SURFACE STATIC PRESSURE COEFFICIENT AT (A) 99% (B) 98.5% (C) 50% SPAN FOR THE CASCADE AT DESIGN INCIDENCE. OPEN SQUARES: EXPERIMENTAL DATA [14]; SOLID LINE: CFD WITH HCSA TURBULENCE MODEL; DASHED LINE: CFD WITH SA TURBULENCE MODEL; DASH-DOTTED LINE: CFD WITH K-Ω SST TURBULENCE MODEL.

The HCSA model results are in good agreement with the experimental results reported by Kang and Hirsch; the detailed experimentally measured total pressure losses can be found in Figure 9 of their paper [14].

The loss coefficient contours enable visualization of the size, intensity, and location of the corner separation. The corner separation size is overestimated by the SA model compared with the HCSA model, and instead of a concentrated region of high loss close to the endwall, the high loss region persists up the span – there is much less three-dimensional structure to the loss contours for the SA model. Comparing these two models' results in more detail, the level of loss predicted by the SA model rises moving away from the endwall, while for the HCSA model the high loss region is confined to the outer span. This explains why the static pressure coefficient is lower than the measured values at all spans in Fig. 3.2 for the original SA model. Figure 3.3 (c) demonstrates that the SST model results are somewhat of a middle ground: the predicted corner separation size is larger than it should be near the endwall, but the loss level decreases moving towards midspan. This is consistent with the increased level of accuracy for the SST model at midspan in Fig. 3.2 compared to near the endwall.

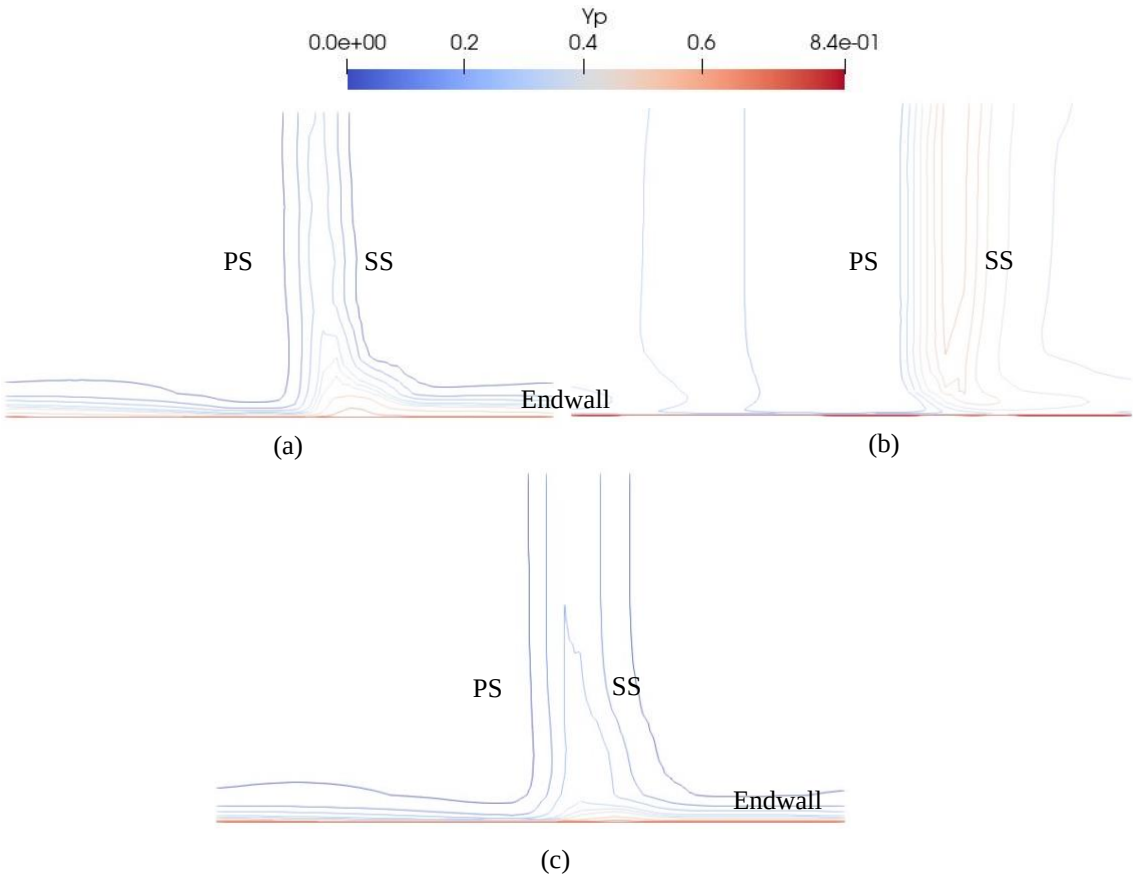

FIGURE 3.3: CONTOURS OF TOTAL PRESSURE LOSSES AT 25% CHORD DOWNSTREAM OF THE TRAILING EDGE. (A) CFD WITH HCSA TURBULENCE MODEL, (B) CFD WITH SA TURBULENCE MODEL, AND (C) CFD WITH K-Ω SST TURBULENCE MODEL.

To determine why the loss coefficient distributions are so different for the three turbulence models, Fig. 3.4 depicts the normalized kinematic turbulent viscosity distribution $\frac{\nu_t}{\nu}$ at the same location as in Fig. 3.3. The most significant difference between the three models is that only the HCSA model captures the concentrated region of high turbulent viscosity associated with the corner (shed) vortex, which was also seen by Kang and Hirsch [14]. The shed vortex located near mid-span, also at a similar spanwise location as observed in the experiment, is a vortex that is neither the trailing shed vortex nor the trailing filament vortex. The specific reason for this concentrated shed vortex is not clear, but Kang and Hirsch speculated it originates from the spiral node point generated by the separation lines on the suction surface. Although the detailed cause of the shed vortex at

mid-span requires further investigation, the HCSA model is able to accurately capture both these regions of high vorticity and turbulent viscosity.

The turbulent viscosity contours also indicate that the SA model predicts the corner separation to be too large and to persist up the span (Fig. 3.4 (a)). The SST model fails to show a distinct vortex core in the turbulent viscosity distribution (Fig. 3.4 (c)), though further from the endwall the distribution is more in line with the HCSA results. We next explore the reasons for the inaccurate predictions by the SA and SST models.

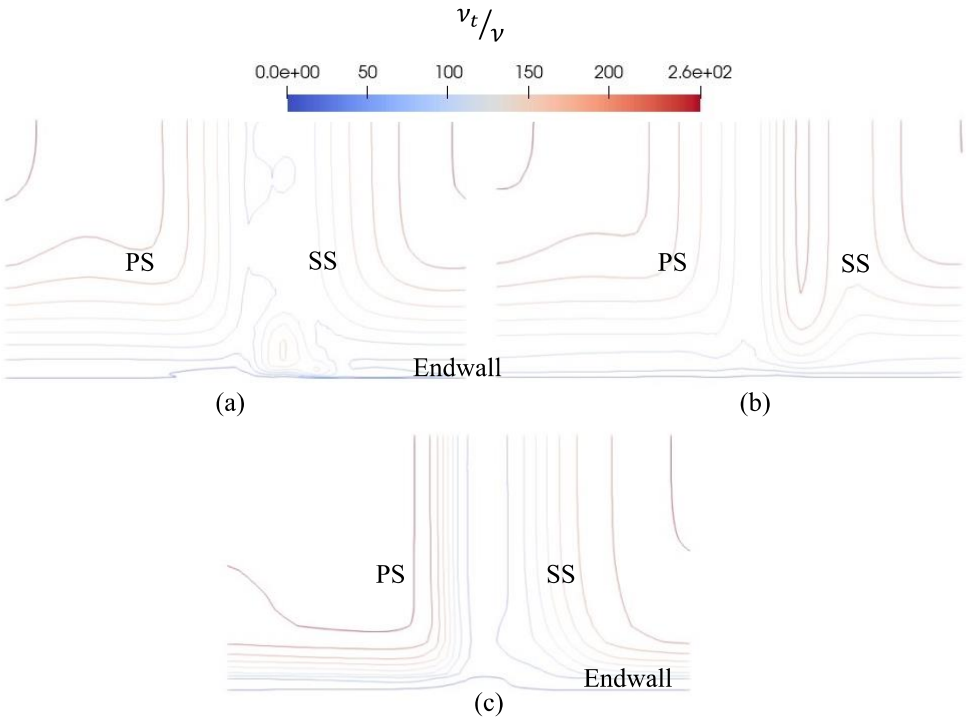

FIGURE 3.4: CONTOURS OF NORMALIZED KINEMATIC TURBULENT VISCOSITY $\frac{\nu_t}{\nu}$ FROM THE ENDWALL TO MID-SPAN AT 25% CHORD DOWNSTREAM OF THE TRAILING EDGE. (A) CFD WITH HCSA TURBULENCE MODEL, (B) CFD WITH SA TURBULENCE MODEL, AND (C) CFD WITH K-Ω SST TURBULENCE MODEL.

From equations 3.4, 3.8 and 3.10, the modifications in the HCSA model compared with the SA model are in the production and dissipation terms of the transport equation, but an investigation of both terms indicates that the production term is the one which looks the most different between the two models. Figure 3.5 (a) and (b) demonstrate the difference of production term between these two models. By introducing the corrected

helicity term, shown in Fig. 3.6, the production term in the HCSA model is able to produce additional turbulent viscosity which aids in keeping the flow attached near the endwall, preventing over-prediction of the corner separation. The helicity correction is significant (compared to 1, the term without correction) in the regions of high production near the endwall.

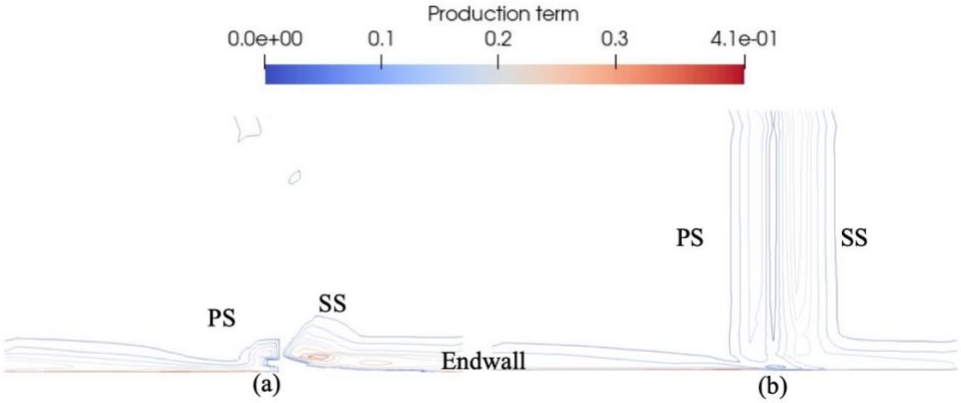

FIGURE 3.5: CONTOURS OF PRODUCTION TERM IN THE (A) HCSA TURBULENCE MODEL AND (B) ORIGINAL SA MODEL FROM THE ENDWALL TO MID-SPAN AT 25% CHORD DOWNSTREAM OF THE TRAILING EDGE.

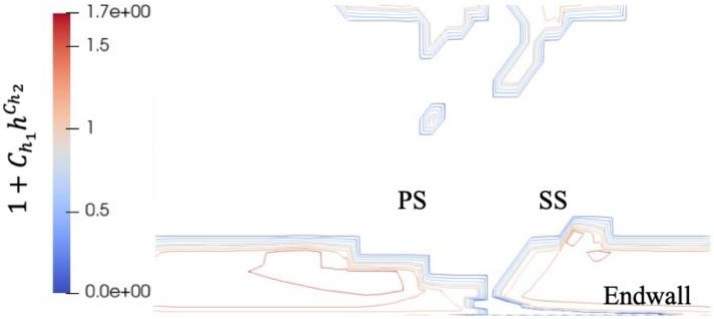

FIGURE 3.6: HELICITY CORRECTION TERM IN THE HCSA TURBULENCE MODEL FROM THE ENDWALL TO MID-SPAN AT 25% CHORD DOWNSTREAM OF THE TRAILING EDGE.

The SST model's calculated specific dissipation rate ω and turbulence kinetic energy k are shown in Fig. 3.7. For the k-ω SST model, the kinematic turbulent viscosity ν_t is calculated as [18],

$$\nu_t = \frac{k}{\omega} \tag{3.17}.$$

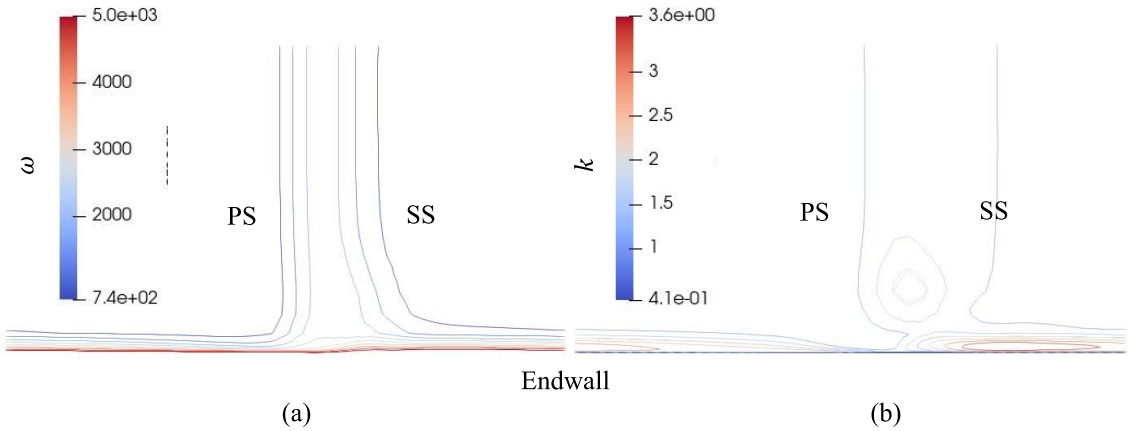

FIGURE 3.7: K-Ω SST TURBULENCE MODEL CALCULATED CONTOURS OF (A) SPECIFIC DISSIPATION RATE AND (B) TURBULENCE KINETIC ENERGY FROM THE ENDWALL TO MID-SPAN AT 25% CHORD DOWNSTREAM OF THE TRAILING EDGE.

The corner vortex is visible in the contours of turbulence kinetic energy, while the specific dissipation rate is distributed nearly uniformly along the span. The spanwise behaviour is thus dominated by k, and it can be seen that while some kind of corner vortex appears to have arisen, leading to reasonable accuracy at 98.5% span in Fig. 3.2, it is located too far away from the endwall, so that the loading at 99% span in Fig. 3.2 is much less accurate. Approaching midspan, the SST model predicts little spanwise variation, and is able to capture the loading correctly. The transport of k thus appears to be responsible for the misplacement of the corner vortex and thus poor prediction of the nature of the corner separation. The more complex model is still not able to capture the interaction between streamwise vorticity and loss generation, while the HCSA model is able to capture this key aspect of the flow in turbomachines.

3.5 Conclusion

In this paper, the HCSA turbulence model from Liu et al. [7] is shown to be correctly implemented in OpenFOAM by validation using a NACA 65-1810 linear cascade for which experimental measurements are available [14]. By comparing the HCSA flow field and turbulence model terms with those of the SA and SST models, some insight into the underlying reasons for the ability of the HCSA model to avoid over-predicting corner separation size is obtained. The SA model is unable to link the local helicity to the turbulent

viscosity production, which leads to premature flow separation. The SST model generally is accurate away from the endwalls, but it also struggles to capture the impact of rotational flow near the endwall, resulting in the corner vortex being too large and causing separation which it should not. These findings support the advantages of the HCSA model for correctly capturing corner flow details in steady RANS computations. By using the swirling flow to produce additional turbulent viscosity, the HCSA model can avoid triggering artificial breakdown of the flow near the endwall in fans and compressors, and this is why it is able to capture the stall point with reasonable accuracy even in steady computations as has been shown by Lopez et al. [8] and Yu et al. [9].

3.6 Nomenclature

Symbols

d	Distance from the wall
h	Normalized helicity
I	Turbulence intensity
k	Turbulence kinetic energy
l	Turbulent length scale
p	Pressure
v	Velocity
ρ	Density
ν	Molecular kinematic viscosity
$\tilde{\nu}$	Modified kinematic turbulent viscosity
ϖ	Vorticity
ω	Specific dissipation rate
ν_t	Kinematic turbulent viscosity
C_p	Blade surface static pressure coefficient
Y_p	Total pressure-based loss coefficient

Subscripts

0	Stagnation quantity
1	Station number (cascade inlet)
2	Station number (25% chord downstream of cascade trailing edge)
LE	Leading edge
TE	Trailing edge
PS	Pressure surface
SS	Suction surface

3.7 References

[1] F. R. Menter, “Two-equation eddy-viscosity turbulence models for engineering applications,” AIAA J., vol. 32, no. 8, pp. 1598–1605, Aug. 1994, doi: 10.2514/3.12149.

[2] P. Spalart and S. Allmaras, “A one-equation turbulence model for aerodynamic flows,” in 30th Aerospace Sciences Meeting and Exhibit, in Aerospace Sciences Meetings. American Institute of Aeronautics and Astronautics, 1992. doi: 10.2514/6.1992-439.

[3] F. R. Menter, “Review of the shear-stress transport turbulence model experience from an industrial perspective,” Int. J. Comput. Fluid Dyn., vol. 23, no. 4, pp. 305–316, Jan. 2009, doi: 10.1080/10618560902773387.

[4] S. Yin, D. Jin, X. Gui, and F. Zhu, “Application and comparison of SST model in numerical simulation of the axial compressors,” J. Therm. Sci., vol. 19, no. 4, pp. 300–309, Aug. 2010, doi: 10.1007/s11630-010-0387-8.

[5] K.-B. Lee, M. Wilson, and M. Vahdati, “Validation of a Numerical Model for Predicting Stalled Flows in a Low-Speed Fan—Part I: Modification of Spalart–Allmaras Turbulence Model,” J. Turbomach., vol. 140, no. 5, Apr. 2018, doi: 10.1115/1.4039051.

[6] S. Kim, G. Pullan, C. A. Hall, R. P. Grewe, M. J. Wilson, and E. Gunn, “Stall Inception in Low-Pressure Ratio Fans,” J. Turbomach., vol. 141, no. 7, Feb. 2019, doi: 10.1115/1.4042731.

[7] Y. Liu, L. Lu, L. Fang, and F. Gao, “Modification of Spalart–Allmaras model with consideration of turbulence energy backscatter using velocity helicity,” Phys. Lett. A, vol. 375, no. 24, pp. 2377–2381, Jun. 2011, doi: 10.1016/j.physleta.2011.05.023.

[8] D. I. Lopez, T. Ghisu, T. Kipouros, S. Shahpar, and M. Wilson, “Extending Highly Loaded Axial Fan Operability Range Through Novel Blade Design,” J. Turbomach., vol. 144, no. 12, Sep. 2022, doi: 10.1115/1.4055350.

[9] Z. Yu, H. Raza, and J. Defoe, “Assessment of fan stall point identification ability of steady RANS computations with the Helicity-corrected Spalart-Allmaras turbulence model,” presented at the ASME Turbo Expo 2023, Boston, Massachusetts: ASME, 2023. doi: GT2023-104039.

[10] OpenCFD Ltd, “OpenFOAM v2206,” ESI OpenCFD Release OpenFOAM® v2206, 2022. https://www.openfoam.com/news/main-news/openfoam-v2206 (accessed Apr. 25, 2023).

[11] C. E. Leith, “Stochastic backscatter in a subgrid-scale model: Plane shear mixing layer,” Phys. Fluids Fluid Dyn., vol. 2, no. 3, pp. 297–299, Mar. 1990, doi: 10.1063/1.857779.

[12] M. Lesieur, Turbulence in Fluids, vol. 84. in Fluid Mechanics and its Applications, vol. 84. Dordrecht: Springer Netherlands, 2008. doi: 10.1007/978-1-4020-6435-7.

[13] Ansys Inc, “Ansys Fluent | Fluid Simulation Software,” 2023. https://www.ansys.com/products/fluids/ansys-fluent (accessed Apr. 25, 2023).

[14] S. Kang and C. Hirsch, “Three Dimensional Flow in a Linear Compressor Cascade at Design Conditions,” presented at the ASME 1991 International Gas Turbine and

Aeroengine Congress and Exposition, American Society of Mechanical Engineers Digital Collection, Mar. 2015. doi: 10.1115/91-GT-114.

[15] S. Kang, "Five-Hole Probe Calibration.," Research report of Fluid Mechanics Department, VUB, 1989.

[16] Autodesk Inc, "AutoCAD Software | Get Prices & Buy Official AutoCAD 2023 | Autodesk," 2022. https://www.autodesk.ca/en/products/autocad/overview?panel=buy&AID=12797027&PID=8206971&SID=jkp_CjwKCAjw9J2iBhBPEiwAErwpedoOIZVPaEpNaxIpz86yrW9lO0Of6pI3CzVUtC7VVwD8smGd_V1OYBoCMb0QAvD_BwE&cjevent=d9aa2341e38411ed8336008e0a82b832&mktvar002=afc_ca_deeplink&affname=8206971_12797027&term=1-YEAR&tab=subscription&plc=ACDIST (accessed Apr. 25, 2023).

[17] A. F. Molland and S. R. Turnock, "Theoretical and numerical methods," in Marine Rudders, Hydrofoils and Control Surfaces, Elsevier, 2022, pp. 297–388. doi: 10.1016/B978-0-12-824378-7.00018-4.

[18] F. Menter, "Zonal Two Equation k-w Turbulence Models For Aerodynamic Flows," in 23rd Fluid Dynamics, Plasmadynamics, and Lasers Conference, Orlando,FL,U.S.A.: American Institute of Aeronautics and Astronautics, Jul. 1993. doi: 10.2514/6.1993-2906.

CHAPTER 4
SUMMARY, CONTRIBUTIONS, AND FUTURE WORK

4.1 Summary

Several applications of the modified SA model have been investigated for compressor/fan behaviour studies, and notably, Kim et al. [1] and Lee et al. [2] carried out URANS computations with the modified SA model that introduces adaptive wall function and includes the effects of an adverse pressure gradient to improve the accuracy of shock wave boundary layer interaction prediction. Also, they tested the steady performance of the modified SA model. They found that the steady-state simulation can predict the stall inception within a small error, indicating the high feasibility of stall prediction by using steady RANS. Recently, most simulations with steady RANS computation are in the compressible flow. The incompressible flow simulation can be used as the low-speed fan and some theoretical stall study since it simplifies the computation process. Getting a convergent result is easier for the steady state than the compressible flow. The primary motivation behind this thesis is the lack of these elements in the literature reviewed for this work.

Chapter 2 presented the fan stall point identification ability of the HCSA model, and the results reveal that the steady RANS computation is able to predict the stall margin in incompressible flow with a 1.2% error by using the HCSA model. The error is only 1% bigger than the URANS simulation. In conclusion, the steady state RANS can make a relatively accurate prediction for stall inception, and if necessary, the exact stall point and stall inception cause can be identified by URANS computation. This way, the computational resources are drastically reduced compared with the large eddy simulation (LES) and the traditional URANS simulations (which would need to start from a higher flow coefficient to ensure a stable start). This chapter also demonstrates that the original SA model overestimates the scale of corner separation and hence causes the stall inception much earlier than observed in experiments. However, the HCSA model predicts that tip leakage at the leading edge is the dominant mechanism of stall inception, in both RANS and URANS, in agreement with experimental data. The fan characteristic map shows an excellent correspondence to the experimental data.

Chapter 3 detailed the verification of the HCSA model's ability to predict corner separation. Compared with the experimental data, the HCSA model predicts the flow separation most accurately among the three turbulence models (HCSA, SA, and SST). Not only the corner vortex is correctly predicted, but the HCSA model also captures the concentrated shed vortex near midspan in a NACA cascade. At the same time, the original SA model overestimates the corner separation, and the SST model underestimates the vortex scale. The introduced helicity correction recognizes the vortex sensitively and can accurately predict the scale of a vortex to avoid it growing too large or decaying too early. Generally, the HCSA model is capable of capturing flow separation and dramatically improves the predicted accuracy of the original SA model.

4.2 Contributions

The major contributions from this thesis can be related to the objectives outlined in section 1.1 as follows:

> **Contribution 1.** Verified the correct implementation of the HCSA turbulence model in OpenFOAM and made the implementation and source code freely available.

The results of HCSA match the experiment conducted by Kang and Hirsch [3], and the comparison among HCSA, SA and SST models reveals that the original SA model will overestimate the flow separation. In contrast, the SST model will underestimate the separation. Only the HCSA model can predict separation accurately in terms of both location and size. The HCSA model implementation instructions and source code are shown in Appendix A.

> **Contribution 2.** Quantified the accuracy of RANS and URANS relative to experiment for fan/compressor stall point prediction in incompressible flow (with the HCSA model).

The computation time is reduced from one to two months for URANS to about one week by adopting the HCSA model in RANS computations. The steady RANS model has a reasonable error at 1.2% for the stall margin (compared to 0.2% for URANS).

Contribution 3. Determined how the HCSA model, in steady RANS, is able to correctly identify the stall point.

The dominant mechanism for stall inception in the fan studied is revealed from URANS to be due to tip leakage flow spillover creating passage blockage. The HCSA model suppresses non-physical corner separation and thus allows the tip leakage flow mechanism to arise in steady RANS, while with the original SA model corner separation causes flow instability at higher flow rates, under-predicting stall margin significantly.

4.3 Future Work

As seen in Chapter 2, the computational domain is 1/10 of the whole annulus, which means there are 18 of 20 rotor passages and 27 of 30 stator passages that are not simulated. The stall propagation across the entire wheel is not verified. Therefore, further simulation can focus on the propagation of the stall cell in the adjacent passage since it is unclear whether the stall cell will grow or decay after several revolutions. What is evident in this studied fan case, is that the stall inception in the tested 1/10 passage causes the blockage in all passages since it matches the full wheel experimental data. However, when the first stall cell generates and whether it affects the adjacent blade are not captured by the URANS simulation performed in this thesis. The reason for the 1% stall margin predicted by the HCSA RANS computations compared to URANS could potentially be related to the small number of rotor blade passages (2) used in this thesis, while in the literature past URANS stall predictions typically use more passages (e.g. 6 in Hewkin-Smith et al. [4]). The impact of the number of passages on the predicted stalling flow coefficient for HCSA RANS computations is thus a useful area of investigation in the future.

4.4 References

[1] S. Kim, G. Pullan, C. A. Hall, R. P. Grewe, M. J. Wilson, and E. Gunn, "Stall Inception in Low-Pressure Ratio Fans," *J. Turbomach.*, vol. 141, no. 7, Feb. 2019, doi: 10.1115/1.4042731.

[2] K.-B. Lee, M. Wilson, and M. Vahdati, "Validation of a Numerical Model for Predicting Stalled Flows in a Low-Speed Fan—Part I: Modification of Spalart–Allmaras Turbulence Model," *J. Turbomach.*, vol. 140, no. 5, Apr. 2018, doi: 10.1115/1.4039051.

[3] S. Kang and C. Hirsch, "Three Dimensional Flow in a Linear Compressor Cascade at Design Conditions," presented at the ASME 1991 International Gas Turbine and Aeroengine Congress and Exposition, American Society of Mechanical Engineers Digital Collection, Mar. 2015. doi: 10.1115/91-GT-114.

[4] M. Hewkin-Smith, G. Pullan, S. D. Grimshaw, E. M. Greitzer, and Z. S. Spakovszky, "The Role of Tip Leakage Flow in Spike-Type Rotating Stall Inception," J. Turbomach., vol. 141, no. 6, Jun. 2019, doi: 10.1115/1.4042250.

APPENDIX A
IMPLEMENTATION OF HCSA MODEL IN OPENFOAM

To implement the modified turbulence model in OpenFOAM v2206, the first step is to create an `src` folder in the user's OpenFOAM project folder. In this folder, create a `TurbulenceModels` folder. In the `TurbulenceModels` folder, create `incompressible` and `turbulenceModels` folders. In the `turbulenceModels` folder, create a `RAS` folder. In the `RAS` folder, createa a `HSpalartAllmaras` folder. Copy the `SpalartAllmaras.H` and `SpalartAllmaras.C` files from the `src/TurbulenceModels/turbulenceModels/RAS/SpalartAllmaras` folder in the OpenFOAM installation folder to the `HSpalartAllmaras` folder. Rename the files `HSpalartAllmaras.H` and `HSpalartAllmaras.C`, respectively. In both files, replace all instances of the string "`SpalartAllmaras`" with "`HSpalartAllmaras`". Edit the `HSpalartAllmaras.C` file's Stilda subroutine as follows:

```
//Modified Stilda
return
(
max
   (
  (scalar(1)+scalar(0.71)*pow(mag((this->U_())&fvc::curl(this-
>U_)().v())/(max
       (mag(this->U_())*mag(fvc::curl(this->U_)().v()),
       dimensionedScalar ("small", dimensionSet(0, 1, -2, 0, 0,
       0),SMALL))
 ),scalar(0.6))
  )*Omega + fv2(chi(), fv1())*nuTilda_()/sqr(kappa_*y_),Cs_*Omega
  )
);
```

Then copy the `turbulentTransportModels.C` file from:

`src/TurbulenceModels/incompressible/turbulentTransport Models` in the OpenFOAM installation folder to the incompressible folder. Rename the file:

`myTurbulentTransportModels.C`. In the file, remove all lines defining specific models, and add in two lines at the end:

```
#include "HSpalartAllmaras.H"
makeRASModel(HSpalartAllmaras);
```

Then copy the `Make` folder and the files it contains from `src/TurbulenceModels/incompressible` in the OpenFOAM installation folder to the `incompressible` folder.

Edit the file `Make/files` in the `incompressible` folder, remove everything and replace with:

```
myTurbulentTransportModels.C
LIB =
$(FOAM_USER_LIBBIN)/libmyIncompressibleTurbulenceModels
```

Edit the file `Make/options` in the `incompressible` folder. Replace the entire file contents with:

```
EXE_INC = \
    -I../turbulenceModels/lnInclude \
    -I$(LIB_SRC)/finiteVolume/lnInclude \
    -I$(LIB_SRC)/meshTools/lnInclude \
    -I$(LIB_SRC)/transportModels \
    -I$(LIB_SRC)/TurbulenceModels/turbulenceModels/lnInclude \
    -I$(LIB_SRC)/TurbulenceModels/incompressible/lnInclude
LIB_LIBS = \
    -lturbulenceModels \
    -lfiniteVolume \
    -lmeshTools \
    -lincompressibleTransportModels \
    -lincompressibleTurbulenceModels
```

Finally, run the two following commands from the `incompressible` folder:

```
wmakeLnInclude -u ../turbulenceModels
wmake
```

To enable the use of the new model, in the `controlDict` file of the case to be run, add the line:

```
libs("libmyIncompressibleTurbulenceModels.so")
```

VITA AUCTORIS

NAME: Zhifan Yu

PLACE OF BIRTH: Nanjing, Jiangsu, China

YEAR OF BIRTH: 1996

EDUCATION: Nanjing Institute of Technology, BASc., Nanjing, Jiangsu, China, 2019

Queen's University, MEng., Kingston, ON, 2020

University of Windsor, MASc., Windsor, ON, 2023